Toward noninvasive monitoring of plant leaf water content by electrical impedance spectroscopy

Ernesto Serrano-Finetti[1], Eduardo Castillo[2], Smith Alejos[3] and L. M. León Hilario[2,3]

[1]Instrumentation, Sensors and Interfaces Group, Universitat Politècnica de Catalunya–BarcelonaTech, C. Esteve Terradas, 7, 08860 Castelldefels (Barcelona), Spain

[2]Facultad de Ingeniería y Arquitectura, Instituto de Investigación Científica, Universidad de Lima, Avenida Javier Prado Este 4600, Santiago de Surco, Lima 15023, Perú

[3]Facultad de Ciencias, Universidad Nacional de Ingenieria, Apartado 31-139, Av. Túpac Amaru 210, Lima, Perú

Corresponding author: lmleon@ulima.edu.pe

Abstract

Plant water content is one key factor that affects the plant wellbeing. Moreover, detecting the plant water needs in a timely manner is important when coming to irrigation strategies (water management). A first step toward plant water monitoring is the availability of a portable and cost-effective system that yields reliable information. Electrical impedance spectroscopy (EIS) has previously been used invasively to provide such data and can be implemented at an acceptable cost. In this work, a cost-effective impedance analyzer has been built capable of performing four-electrode noninvasive measurements. Besides, data fitting has been improved by using a modified equivalent circuit model, yielding relevant information about the plant water status. The results show that the resistance modelling the extracellular fluid can track the change in water content of a plant leaf while it is drying at room temperature. On the other hand, impedance data might provide information about the leaf tissue structure at small inter-electrode distances.

Keywords: Plant electrical properties; electrical impedance spectroscopy; plant water content.

1. Introduction

Water resources are becoming scarce in most countries around the world. This makes the task of allocating those resources for agricultural production increasingly difficult (Kalyanaraman et al., 2022). However, plant hydration is one of the main factors that determines its wellbeing and yield hence efforts must be made to establish appropriate watering schedules. Sensing technologies and algorithms are currently being developed to help in detecting plant water stress (Elsherbiny et al., 2022), which combined with the experience of farmers constitute a powerful tool for establishing irrigation needs and optimizing water management.

Hydric stress occurs mainly during the drought period and manifests as visible color and structural changes –decrease in turgor, for example. One way to assess the hydric status of a plant is to measure its relative water content (RWC) (Zimmermann et al., 2008). The gold standard method (Smart and Bingham, 1974) relies on mass measurements at different leaf sample hydration states: fresh, water-saturated (full turgor) and oven-dried. The process is thus time-consuming –4 to 24 h of water saturation and 24 h of desiccation in the oven, typically– even if one obviates the drying process. It also requires cutting the leaves specifically, adding up to the complexity of the process. Moreover, this method does not allow measuring leaf RWC in vivo or in situ. Therefore, noninvasive methods have been proposed that involve contact and non-contact solutions. Near-infrared spectroscopy (NIRS) is an indirect measurement technique that correlates to RWC to an acceptable degree (Hunt et al., 1987; Torres et al., 2019) and can provide fast in situ estimates. However, the cost of most NIRS equipment is currently very expensive and limits its deployment as a daily use tool in crop maintenance. Alternatively, turgor can be directly measured on the plant leaves (Zimmermann et al., 2008) with very high precision, and relatively low cost.

Electrical impedance measurement is an inexpensive, easy to build, noninvasive technique that provides information about the composition of biological media like plants (Jócsák et al., 2019). A sinusoidal excitation source (a current or a voltage) at a specific frequency is applied onto the biological medium by means of two electrodes attached to its surface. This creates a current flow inside the biological medium and a voltage response is developed and read either at the same injecting electrodes (two-electrode technique) or at a second set of electrodes placed conveniently (four-electrode technique). The magnitude of the current injected into the medium is usually very well below 1 mA. Bathroom scales that provide information about a person's body composition use this technique, calculating the total body water content from a single frequency measurement and empirical formulae to estimate other parameters like fat and muscle content.

Electrical impedance spectroscopy (EIS) uses the same setup to perform a frequency sweep, yielding an impedance spectrum that fits into an equivalent electrical circuit consisting of passive electrical elements (i.e. resistors capacitors). These circuit elements provide information about the electrical properties of the sampled biological medium: the cell membrane electrical capacitance and the intracellular and extracellular water conductivities (Pethig and Kell, 1987). In this way, the plant's physiological activity or structural changes can be tracked as long as it affects its electrical properties. EIS has been used to investigate the water content of roots and stems in potatoes and alfalfa (Hayden et al., 1969). More recently, it has been used to investigate the leaf water content (LWC) with two small electrodes (Barbosa et al., 2022) and found a high correlation between LWC and the impedance magnitude, but the use of two electrodes might have masked the identification of the circuit elements as it was not possible to extract the cell capacitance data nor the intracellular resistance. In such two-electrode measurements, the electrode impedance constitutes an interfering quantity, a problem remediated using the four-electrode technique. Other EIS applications include the plant's response

to environmental changes (Garlando et al., 2022), to different growth and stress conditions (ben Hamed et al., 2016), and to different plant water status (Jamaludin et al., 2015). It has also been used to track the response to nitrogen nutrition stress in tomatoes (Li et al., 2017), and the thermally-induced structural changes in spinach (Watanabe et al., 2017), to name some examples.

Data interpretation and comparison between studies is, to some extent, difficult, as the measurement protocols are mostly ad hoc. The electrodes used were different in their construction –shape and material– and in their degree of invasiveness –surface electrodes vs. inserted needle electrodes. Additionally, the electrodes were placed at very dissimilar locations (leaves or stems, or a combination), making the data interpretation difficult. For example, (Zhang and Willison, 1993) inserted two thin needle electrodes into plant leaf samples –causing damage to the leaves– while (Jamaludin et al., 2015) use two surface electrocardiogram electrodes attached to plant leaves to measure the impedance in vivo. In both cases, it was expected that the electrode impedance interfere with the leaf impedance at the lower frequency range (hundreds of hertz range) but in the work by Zhang and Wilson the insertion reduced this problem. However, the observed values were in the kiloohm to tens of kiloohm range. These values are orders of magnitude larger than those obtained by (Comparini et al., 2020) at dc, where the electrodes were inserted into the stem of an olive tree plant in vivo, yielding values in the ohms to hundred ohms range. Although in these studies the measured values were quite dissimilar, they all indicated an increase in impedance with decreased plant water content.

Wide acceptance of EIS as a technique to estimate the RWC is limited by two factors: i) the high cost and bulk of most commercial impedance analyzers, and ii) the accuracy of the measurement. For benchtop studies, the necessary frequency range will usually go from around 10 Hz to 1 MHz, although some studies report promising results with lower frequency ranges. This is the case of own-

built portable impedance analyzers based on commercially available integrated circuits like the AD5933 (Analog Devices, Inc.) used to detect fruit ripening (Ibba et al., 2021). (Jamaludin et al., 2015) also used this device, but the results were inconclusive as the impedance spectrum exhibited low frequency values exceeding the AD5933 specifications, preventing the fit to an equivalent circuit. Nonetheless, from 70 kHz to 100 kHz, the impedance magnitude showed a significant correlation with RWC.

In this work, a EIS measuring system has been implemented that is based on a low-cost USB acquisition and generation system –the Analog Discovery 2 (AD2)– and a simple analog front-end (AFE). The proposed system performs four-electrode impedance measurements in the frequency range from 100 Hz to 1 MHz. This setup avoids the influence of electrode polarization that usually arises when using two electrodes to measure the impedance. Leaf samples of *spinacea oleracea L.* were prepared and their impedance measured and fitted to an equivalent circuit. Tests were performed to assess the influence of electrode positioning and the capability of the system to track water loss during the spontaneous drying of the leaf samples.

2. Materials and methods

In this section, a novel measurement system able to acquire the impedance spectrum of a leaf in the 100 Hz - 1 MHz range is described. It uses four surface electrodes to prevent the interference of the electrode impedance.

2.1 EIS measurement system

Figure 1A shows a block diagram of the proposed EIS system. It comprises an AD2 and a fully-differential AFE. Briefly, the AD2 has two differential input channels, CH1 and CH2 (14-bit resolution, 100 MSPS sample rate and 30 MHz analog bandwidth), two 14-bit single-ended waveform generators V_1 and V_2 that can be arranged to create a fully-differential waveform generator –12 MHz maximum frequency– and a programmable power supply, fixed at ±5 V. This fully-differential architecture was chosen to avoid issues with interfering signals that usually manifest as unwanted common-mode signals superimposed onto the impedance voltage response.

A reference resistor R_{sh} and the plant leaf impedance Z_x form a voltage divider. V_1 and V_2 are two synced sine waves of constant amplitude (1 V) that have a relative phase of 180°. V_1- V_2 is thus used as the fully-differential excitation source. Electrodes I_1 and I_2 are the current injection electrodes and E_1 and E_2 are the voltage pick-up electrodes –reading the voltage response from the plant. A_1 and A_2 are two identical AD8066 op amps (Analog Devices, Inc.) configured as a non-inverting fully-differential amplifier with a differential gain G_d = 3 (Figure 1B) fixed by of 499-Ω resistors –as specified by the op-amp manufacturer. At this gain, the AD8066 has a -3 dB bandwidth well exceeding 10 MHz hence its gain and phase deviations are expected to be negligible. However, the AD8066 has a very high input impedance that avoids voltage-loading effects due to the high leaf electrical impedance. In a voltage divider, the reference resistor is usually chosen to be of similar magnitude to the unknown impedance thus R_{sh} is 30 kΩ, which falls within the expected leaf impedance range and is used to measure the current flowing into the leaf. Assuming that the electrode impedance does not surpass 10 kΩ, a range of Z_x from 10 kΩ to 100 kΩ will produce a current between 33 μA and 13 μA. These are very low amplitude currents hence common-mode interfering signals may distort the impedance spectrum. By using a fully differential architecture, these interfering signals should not introduce significant deviations. Smaller currents can also be measured, i.e., when the leaf begins to dry and its impedance surpasses 100 kΩ, but then the impedance spectra might be more susceptible

to electromagnetic interferences and/or noise. Channel 1 of the AD2 is used to read the voltage drop at R_{sh} (V_{CH1}) and Chanel 2 measures that of Z_x (V_{CH2}).

By applying Ohm's law, the impedance magnitude $|Z_x|$ and phase $\angle Z_x$ will be

$$|Z_x| = R_{sh}\frac{|V_{CH2}|}{|V_{CH1}|} \quad (1)$$

$$\angle Z_x = \angle V_{CH2} - \angle V_{CH1} \quad . \quad (2)$$

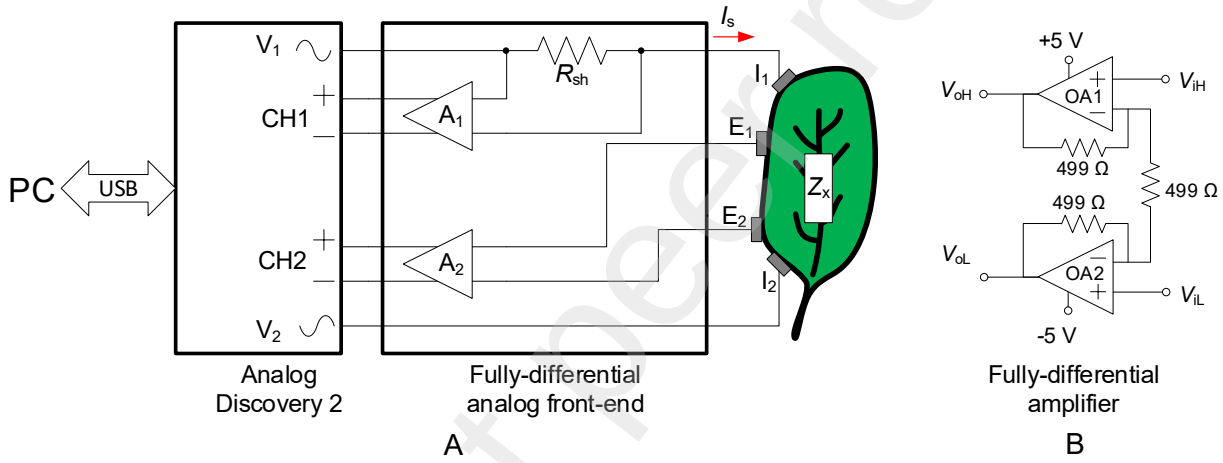

Figure 1. A) Block diagram of the proposed EIS measurement system, showing its two main components: the implemented AFE and the AD2, controlled by a laptop PC. B) Schematic of the fully-differential amplifier design used in A_1 and A_2, that is based on two AD8066 op amps (OA1 and OA2).

An acquisition and control virtual instrument was developed in LabVIEW (National Instruments Corp.). V_{CH1} and V_{CH2} were digitally processed to compute the amplitudes and phases in (1) and (2) with LabVIEW's in-built tone detection block based on a fast-Fourier transform computation, making it unnecessary to demodulate the signals from V_{CH1} and V_{CH2}. In this work, a logarithmic frequency sweep of 101 points between 100 Hz to 1 MHz was used, but this can be easily reprogrammed as long as the frequency does not fall outside the 10 Hz to 10 MHz range (10 MHz is the maximum imposed by the AD2, but the AFE performance at such high frequency will be poor). The system was calibrated

with a 30 kΩ resistor whose reference magnitude and phase values were measured with a 4294A impedance analyzer (Agilent Technologies) in the frequency range from 100 Hz to 1 MHz.

2.2 Impedance spectrum data fitting

Biological tissues exhibit an impedance spectrum with clearly distinguishable dielectric dispersion regions, which are the frequency-domain counterpart of the time-domain relaxation processes. In animals, the small cell sizes (typically up to 100 μm) yield three dispersion regions: α, β, and γ. The β dispersion occurs at a frequency specific to the tissue under test and is linked to the cell membrane. The frequency range below and above this dispersion yields information about the intracellular and extracellular ionic contents. Figure 2A shows the equivalent circuit of a single dispersion tissue that models the possible current flow paths. There, Z_{CPE} is the membrane impedance modeled by a constant phase element; R_{ECF} and R_{ICF} model the extracellular fluid and the intracellular fluid, respectively. Figure 2B is an equivalent circuit derived from the Cole-Cole empirical equation:

$$Z(\omega) = R_\infty + \frac{R_0 - R_\infty}{1 + (R_0 - R_\infty)(j\omega)^\alpha C} = R_\infty + \frac{\Delta R}{1 + (j\omega)^\alpha \Delta RC} \tag{3}$$

where $\Delta R = R_0 - R_\infty$, R_0 is the impedance at zero frequency and R_∞ is the impedance at infinite frequency. The models in Figure 2A and Figure 2B yield equivalent information about the single dispersion. To derive (3) a constant-phase element (CPE) has been used and whose impedance is described by

$$Z_{\mathrm{CPE}} = \frac{1}{(j\omega)^\alpha C}, \tag{4}$$

where α and C are empirical constants that allow good data fitting. The CPE represents an imperfect capacitor, or pseudo-capacitor. Here, C represents the cell-membrane pseudo-capacitance and α is interpreted as a parameter accounting for the dispersion of cell sizes. α is an intrinsic tissue

parameter and is independent of the sample geometry –unlike resistors and capacitors– and has been suggested as a parameter to classify tissues or tissue status.

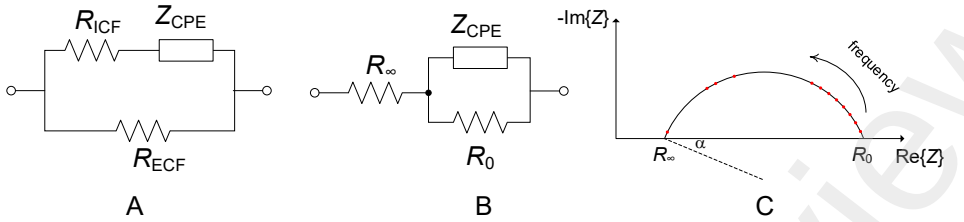

Figure 2. A) Equivalent circuit of an animal cell with a simple dispersion, as derived from the possible current paths. B) Equivalent circuit derived from the Cole-Cole equations. C) Cole-Cole impedance plot showing a depressed semicircle corresponding to either of the equivalent circuits.

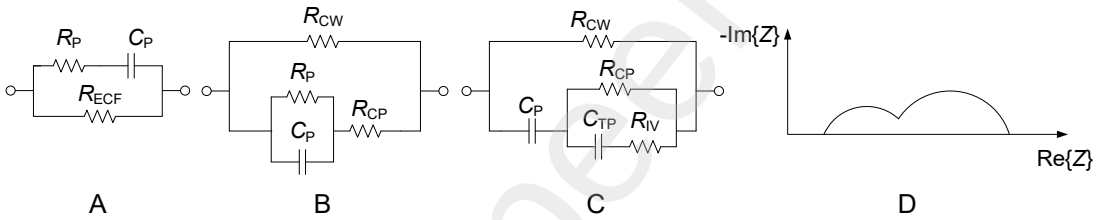

Figure 3. Equivalent circuits for plant tissues: A) Single-shell model, where P stands for plasma (cell wall and membrane); B) Hayden model, where CW stands for the cell wall, CP for the cell cytoplast. C) Double-Shell model, where TP stands for the vacuole tonoplast and IV for the inner vacuole. D) Cole-Cole impedance plot showing a double semicircle, as expected in a double-shell model.

In plants, the cell size is larger (typically up to 300 μm) and the dispersion regions move toward lower frequencies compared to animal cells. Additionally, plants exhibit a somewhat different structure as they have a cell wall besides a cell membrane. Besides, plant cells have large vacuoles that can occupy more than 80% of the total cell volume. The result is that, when drawing the Cole-Cole plots, they may exhibit a double arc, and the fit to single-dispersion circuits is not good. Instead, circuits that are more complex are used: the single-shell model, the Hayden model, or the double-shell model (Prasad and Roy, 2020). The latter exhibits a double arc in the Cole-Cole plot, while the former exhibits only one, as in animals. Double arcs appear in plant protoplasts (Asami et al., 1996),

roots (Repo et al., 2005) and leaves (Zhang and Willison, 1993). However, in some cases, only one visible arc is displayed and the single-shell or Hayden equivalents are a suitable choice. One downside of such circuits is that, usually, the plotted arcs are displaced downwards, meaning that a CPE might be a better choice than capacitors.

In this work, a modified double-shell model was used, where the capacitors in Figure 3C were replaced with CPEs as shown in Figure 4. These CPEs are Z_P, modelling the plasma impedance, and Z_{TP}, modelling the tonoplast impedance. Their expressions are

$$Z_P = \frac{1}{C_P (j\omega)^{\alpha_P}} \tag{5}$$

$$Z_{TP} = \frac{1}{C_{TP} (j\omega)^{\alpha_{TP}}}. \tag{6}$$

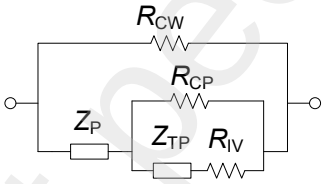

Figure 4. Modified double-shell model where the capacitors are replaced with CPEs: Z_P is the plasma CPE and Z_{TP} is the tonoplast CPE.

As with the series Cole-Cole equations, each CPE associates with a set of resistances, modeling a specific relaxation process. At low frequencies, Z_{TP} is an open circuit and the associated plasmatic membrane characteristic frequency f_P will be

$$f_P = \frac{1}{2\pi \left[\left(R_{CP} + R_{CW} \right) C_P \right]^{\frac{1}{\alpha_P}}}. \tag{7}$$

On the other hand, at high frequencies, Z_P is shorted, and the tonoplast characteristic frequency f_{TP} will be

$$f_{\mathrm{TP}} = \frac{1}{2\pi\left[\left(R_{\mathrm{IV}} + R_{\mathrm{CP}} \,||\, R_{\mathrm{CW}}\right) C_{\mathrm{TP}}\right]^{\frac{1}{\alpha_{\mathrm{TP}}}}}. \tag{8}$$

In the case of a modified single-shell model where C_{p} is replaced with a CPE modelled by (5), the characteristic frequency f_{c} will be

$$f_{\mathrm{c}} = \frac{1}{2\pi\left[\left(R_{\mathrm{P}} + R_{\mathrm{ECF}}\right) C_{\mathrm{P}}\right]^{\frac{1}{\alpha_{\mathrm{P}}}}}. \tag{9}$$

The open-source ZFit MATLAB script (Dellis, 2022) for fitting data to the equivalent circuit has been used to implement the data fitting to this modified model.

2.3 Instrument calibration

Usually, impedance measurement systems need calibration to correct for deviations in magnitude and phase. This was performed using a reference resistor of 1000 Ω whose magnitude and phase were measured with a 4294A impedance analyzer (Agilent). After calibration, a test impedance (Z_{t}) consisting of a 1-kΩ resistor in parallel with a series combination of another 1-kΩ and a 10-nF capacitor was measured with the proposed system. The results were compared with those obtained with the 4294A impedance analyzer.

2.4 Influence of electrode positioning on the measured impedance spectrum

The current injecting and voltage pick-up electrodes were built from thin aluminum foil, forming narrow rectangles. 8-cm square samples were cut from fresh *spinacea oleracea L.* Electrodes I_1 and I_2 were placed at the upper face extremes, while electrodes E_1 and E_2 were placed at the same face, as shown in Figure 4. To decrease contact impedance, a small quantity of ECG gel was spread at the

interface between the leaf and each electrode. Five distances *d* between electrodes were tested: 0,5 cm, 1 cm, 1,5 cm, 2 cm and 2,5 cm. The tests were repeated but with electrodes I_1 and I_2 placed at the lower face, while electrodes E_1 and E_2 were placed at the upper face, and the same distances (*d)* were tested again, totaling 10 different measurements.

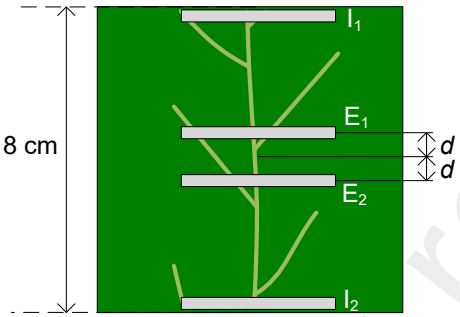

Figure 4. Electrodes were placed onto the square leaf samples at different distances (*d*) between E_1 and E_2.

2.5 Monitoring of the leaves during free drying

Three rectangular leaf samples of 5 cm × 10 cm, all from different *spinacea oleracea L.* plants, were left to dry spontaneously in a closed room with temperatures around 26° and relative humidity in the 70%- 80% range. The electrodes used were placed in the upper face, with *d* = 2 cm. Each leaf sample was placed on an electronic weighing scale (PCE-BS-300, PCE Instruments) with all the measuring electrodes in place. This weighing scale has an accuracy of ±0,03 g over a full scale of 300 g. The loss of weight of each leaf and its complex impedance spectrum were measured simultaneously at 6 different times during two days:

- Day1: initial measurement (t0), and after 3 h (t1) and 6 h (t2)
- Day 2: after 24 h (t3), 27 h (t4) and 30 h (t5)

RWC is a method based on weight loss during desiccation, with the underlying hypothesis that the only mass loss is that due to evaporated water. Here, it was assumed that the progressive mass loss during the free drying process was also due mostly to the water lost. Therefore, the approach used

here was to compare the trends of the equivalent-circuit parameter values against the leaf sample weight during the drying process to identify those who are more sensible to water content loss.

3. Results and discussion

3.1 System calibration

The results of the magnitude and phase spectrum of Z_t before and after calibration are shown in Figures 5a and 5b, respectively, and those obtained with the 4294A impedance analyzer are shown in Figure 6. The frequency range was extended up to 10 MHz, although the intended frequency range ends at 1 MHz. At 100 Hz, the reference measurements –obtained with the commercial impedance analyzer– were 1001 Ω/-0,1 ° (magnitude/phase), while at 1 MHz they were 503 Ω/-0,1 °. Before the calibration, the values obtained with the proposed system were 994 Ω/-0,3 ° at 100 Hz, and 502 Ω/-1,8 ° at 1 MHz. Those values changed after calibration to 1001 Ω/-0,2 ° at 100 Hz, and to 501 Ω/0 ° at 1 MHz. The minimum phase occurred at 11,7 kHz with the reference instrument, at 12,4 kHz with the proposed system before calibration and at 12 kHz after calibration. These measurements confirm that this low-cost system can provide reliable data in the frequency range from 100 Hz to 1 Mhz.

At frequencies larger than 1 MHz the largest deviations observed are in the phase spectra (5 ° larger with the proposed system, at 10 MHz). This large phase error means that this system will not be able to yield reliable data above 1 MHz.

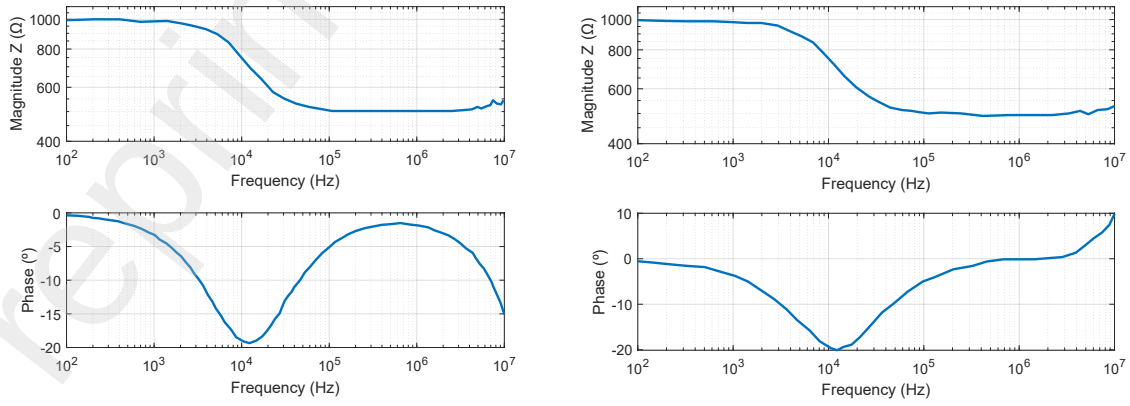

A B

Figure 5. Impedance spectrum (magnitude and phase) of Z_t measured with the proposed system a) before calibration an b) after calibration.

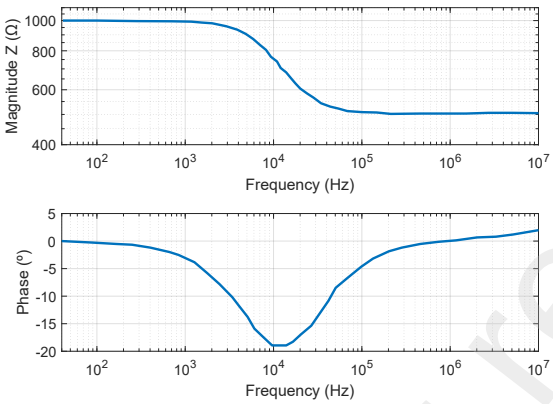

Figure 6. Impedance spectrum (magnitude and phase) of Z_t obtained with the 4294A impedance analyzer.

3.2 Electrode positioning

The Cole-Cole plots for the measured impedances at different *d* values are displayed in Figure 7, where the upper plot corresponds to I1 and I2 placed at the upper leaf face (UF in Table 1) and the lower plot corresponds to the same electrodes placed on the lower leaf face (LF in Table 1). E1 and E2 were always placed on the upper leaf face. The fitted electrical parameters of the double-shell model are shown in Table 1. At *d* = 0,5 cm, the Cole-Cole plot exhibits two depressed arcs (Figure 8) and the fitted values are generally in agreement with those obtained by (Zhang and Willison, 1993) for cabbage leaves (*brassica oleracea*). Using CPEs instead of capacitors improved data fitting.

According to the equivalent circuit used, the high frequency arc (HFA) –to the left of the plot– depends on the smaller structures formed by the vacuoles and its membrane –the tonoplast–, while the cell wall and the cytoplasm originate the lower frequency arc (LFA) –to the right of the plot. The resistive elements increased with *d* while the capacitive elements decreased. These changes are

mostly due to geometrical changes: losing water shrinks the cells and vacuoles, hence the membrane surface decreases, and the conductive paths narrow.

The LFA is wider than the HFA at the smallest *d*, although the frequency range did not permit to see a complete LFA because f_P is around 22 Hz. Because these values of the characteristic frequencies fall outside the measurement range, they are considered unreliable. However, this feature also points to the possibility of better discrimination of finer structures. When increasing *d*, the HFA becomes more and more dominant and f_P and f_{TP} move close together, making their discrimination difficult. At larger scales –larger *d* values– the α_P value increases. One interpretation of α_P in a CPE is that it a low value indicates a broader dispersion in cell size distribution. Hence, an increase is a sign that the material becomes homogeneous at a "large" scale. However, α_{TP} shows little change with *d*, possibly due to the fact that vacuoles occupy a large fraction of the epidermis cells (89 %) and of the mesophyll cells (79 %) (Winter et al., 1994), and do not show large variations if the turgor is uniform across the leaf, independently of the cell sizes. A second observation is that the HFA arc is dominant at the larger *d* values, hence if vacuole water is lost it will be better detected for those *d* values, and the LFA arc would become less important.

In (Watanabe et al., 2017), *spinacea oleracea L.* leaves were thermally treated to investigate the capability of EIS to track structural changes –mainly geometrical– in the leaves after thermal and mechanical treatments. There, the replacement of CPEs instead of capacitors in the Hayden model – similar to this study– also led to good fitting results. The findings of that study also showed impedance changes correlated with the structural changes induces by the thermal treatments applied to the leaf samples.

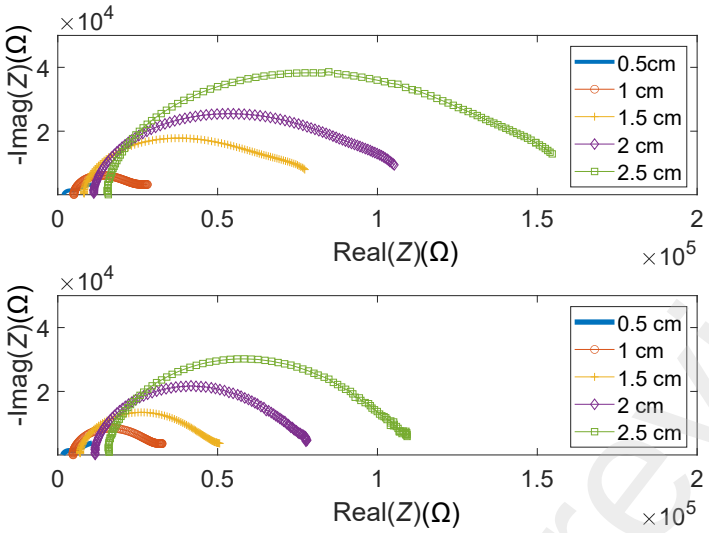

Figure 7. Cole-Cole plots for the measured and fitted data at different distances *d*. The upper plot displays data measured with I_1 and I_2 at the upper leaf face, while the lower plot is for the lower face.

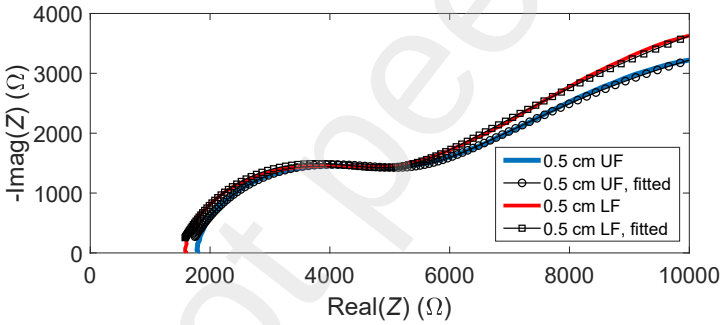

Figure 8. Cole-Cole plot for the measured and fitted impedance data at *d* = 0.5 cm and with the injecting electrodes at both faces of the leaf.

The parameter values are not significantly different in both the UF and LF electrode setups (Table 1). The implication is that the electrodes can be placed as deemed necessary to best fit the leaf dimensions.

Data interpretation of the four-electrode impedance measurements depends also on geometrical considerations. The current density paths between injecting and pick-up electrodes determine the

sensitivity to the material impedance throughout the volume conductor and might create small regions of zero impedance and even negative impedance that contribute to the overall measured impedance (Grimnes and Martinsen, 2015). In (Zhang and Willison, 1993), the two-electrode technique was used with electrodes inserted into the leaf, causing damage but lowering the contact impedance, which can be large at low frequencies –masking the LFA–. But the two-electrode does not have the problems of sensitivity of the four-electrode technique. In contrast, using four electrodes largely attenuates the issues introduced by the electrode contact impedance, enabling noninvasive measurements. The influence of the sensitivity in the measurements has not been considered in this work, and is left for future research.

Table 1

Fitted parameters of the impedance data for all positions, as described in section 2.3. The parameters correspond to the double-shell equivalent circuit in Figure 3C. UF stands for the upper leaf face and LF for the lower leaf face.

d (cm) - I_1&I_2	R_{cw} (kΩ)	R_{CP} (kΩ)	C_P (μF)	α_P	R_{IV} (kΩ)	C_{TP} (nF)	α_{TP}	f_P (Hz)	f_{TP} (kHz)
0,5-UF	24,88	5,40	3,288	0,47	2,35	9,99	0,79	21,9	25,5
1,0-UF	33,26	58,16	0,162	0,60	4,93	8,34	0,73	173,6	5,1
1,5-UF	85,23	116,11	0,025	0,67	6,71	7,79	0,70	443,2	3,1
2,0-UF	114,27	174,17	0,014	0,68	9,41	6,38	0,70	562,2	2,4
25-UF	164,43	262,42	0,007	0,71	12,84	4,55	0,70	588,6	2,1
0,5-LF	28,11	5,01	3,182	0,48	2,03	9,47	0,79	17,0	28,9
1,0-LF	40,67	86,44	0,137	0,64	4,19	6,67	0,74	92,0	3,7
1,5-LF	55,51	218,01	0,028	0,71	5,95	5,41	0,72	158,3	1,7
2,0-LF	82,24	328,64	0,006	0,75	10,78	2,97	0,75	492,6	1,6
2,5-LF	114,37	480,64	0,004	0,76	14,45	2,48	0,74	451,8	1,3

363 3.3 EIS measurements during leaf drying

364

365 Figures 9a, 9b and 9c show the Cole-Cole plots of the impedance spectrums of the three leave samples
366 during the drying process, at the times specified in section 2.5. All of them show one dominant arc
367 that corresponds to the HFA, as expected from the results obtained in section 3.2 with *d* values above
368 1,5 cm. For any of the leaves, the maxima of all arcs shows increases (an increase in the impedance
369 magnitude) as the leaf losses water, and its location moves toward the right (lower frequencies).
370 Because there is a dominant arc, a modified single-shell model (Figure 3A) was used. Table 2 shows
371 the fitted values for R_P, R_{ECF}, α_P, C_P, f_c, and the leaf mass m, where f_c is calculated according to (9), and
372 Table 3 shows the results from the linear regression analysis. From the latter, the parameters, R_{ECF}
373 and f_c show a consistent and strong linear correlation with m throughout all the leaf samples, but of
374 opposite sign. R_{ECF} showed R^2 values from 0,897 to 0,998 and increased with m. This behavior is
375 compatible with a loss of weigh due to water evaporation because the leaf becomes less electrically
376 conductive. On the other hand, this same behavior explains why f_c decreases –it is inversely
377 proportional to R_{ECF}– and keeps a consistent trend among the three leave samples.

378

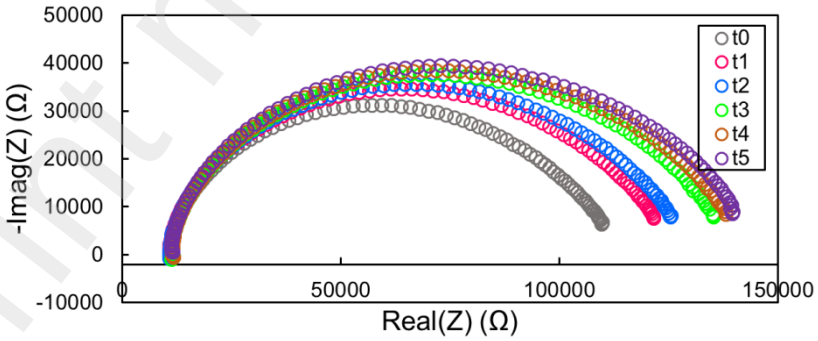

379

380 A

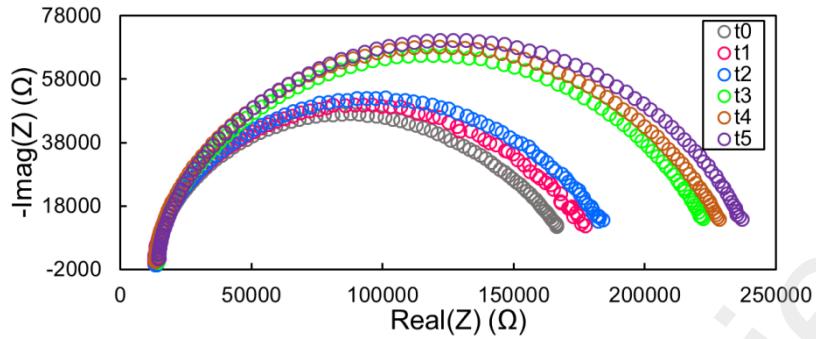

381

382 B

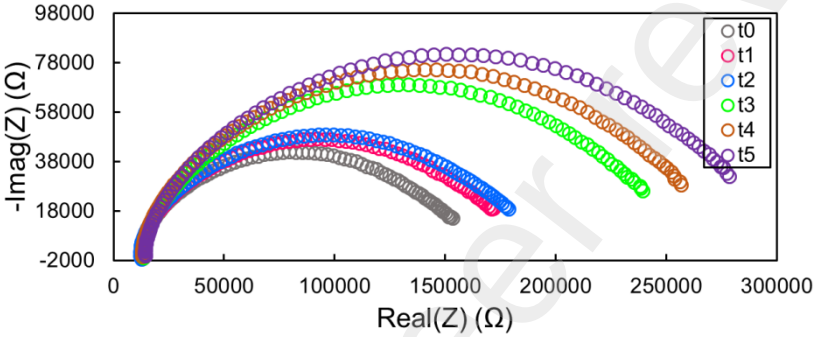

383

384 C

385 **Figure 9**. Cole-Cole plots for the impedance data recorded from the three leaf samples (A, B and C) during the drying

386 process.

387

388 **Table 2**

389 Fitted parameters (R_{ECF}, R_P, C_P, α_P, and f_c) obtained from the three leaf samples (A, B, and C) while they were drying over

390 two days at times t0 to t5, and the corresponding measured leaf mass m.

Sample	Time	R_{ECF} (kΩ)	R_P (kΩ)	C_P (nF)	α_P	f_c (kHz)	m (g)
A	t0	111,76	6,93	5,23	0,69	46,92	5,08
	t1	124,91	6,31	5,88	0,68	39,99	5,02
	t2	129,03	6,26	6,00	0,67	38,43	4,98
	t3	138,55	6,25	6,77	0,66	33,54	4,71
	t4	141,82	6,08	6,84	0,66	33,06	4,66
	t5	144,67	5,68	6,75	0,66	32,83	4,63
B	t0	169,30	7,23	4,98	0,67	34,94	4,49
	t1	179,66	6,82	5,13	0,67	31,98	4,45
	t2	188,75	6,63	5,08	0,67	32,41	4,42
	t3	229,94	7,44	3,67	0,68	30,20	4,28
	t4	235,88	6,58	3,38	0,69	30,18	4,25
	t5	245,33	7,45	3,37	0,68	30,28	4,23
C	t0	157,94	7,25	8,59	0,65	24,74	4,52
	t1	178,65	6,86	9,31	0,64	20,40	4,46
	t2	186,58	5,97	9,59	0,63	20,58	4,43
	t3	254,28	6,85	6,91	0,65	16,73	4,26
	t4	274,12	5,91	6,41	0,65	16,06	4,22
	t5	298,65	6,64	6,24	0,65	15,27	4,2

Table 3. Linear regression analysis results for the fitted parameters on the three leaf samples (A, B, and C). R^2 is the regression coefficient and Trend indicates whether there is a clear increase or decrease of a specific parameter with *m*.

Sample	*m* vs.	R^2	Trend
A	R_{ECF}	0,897	decrease
	R_P	0,64	increase
	C_P	0,913	decrease
	α_P	0,905	increase
	f_c	0,85	increase
B	R_{ECF}	0,999	decrease
	R_P	0,061	-
	C_P	0,939	increase
	α_P	0,786	decrease
	f_c	0,819	increase
C	R_{ECF}	0,985	decrease
	R_P	0,167	-
	C_P	0,825	increase
	α_P	0,364	decrease
	f_c	0,934	increase

R_p is usually interpreted as the intracellular content of the plant cells, and was expected to also show an increase due to water loss that was not confirmed experimentally. On the other hand, C_p was expected to decrease with water loss due to cell shrinking but, again, was not confirmed in these experiments. Possible damage on the cell membrane or in the vacuole membrane might provide an explanation for this behavior, but in this work there were no microscope evidence and the hypothesis cannot be further tested. Lastly, the small variations of α_P around a value of 0,6 might indicate that

the drying process does not increase or decrease the cell size dispersion and is not sensible enough to provide information about water loss.

Other studies have attempted to measure the effect of watering or water stress in plants, but most of them do so at the plant stem, like (Comparini et al., 2020), (Bar-On and Shacham-Diamand, 2021) or (Garlando et al., 2022), that has a completely different geometry: a thicker volume and higher water content due to the plant sap. Therefore, the recorded impedances in those studies were lower as compared to this work. The study by (Bar-On and Shacham-Diamand, 2021) also used the four-electrode technique and recorded the plant weight on a gravimetric platform. Observed increases of the impedance corresponded to weight loss while watering events decreased it. In addition, an ad hoc equivalent circuit was proposed where the resistive components increased with water restriction and stress, which is compatible with the observed behavior here. Regarding the capacitance and exponential of the CPEs, no data was shown, making it difficult to make further comparisons. In (Comparini et al., 2020), two electrodes were inserted into the stem and only the resistance values were reported during stress and watering events, showing the same trend in resistance as in this study. Finally, (Garlando et al., 2022) studied the Bode plots of the impedance and chose a frequency of around 10 kHz to record impedance changes, again confirming the same behavior.

4. Conclusions

A cost-effective impedance analyzer for plant leaves was built. It was tested over a range frequency between 100 Hz and 1 MHz frequency range, demonstrating its capability to perform reliable four-electrode impedance measurements. The electrodes used are very simple and cheap and can be used for noninvasive measurements. It has a simple architecture yet it yields a good quality impedance spectrum for plant leaves due to its fully-differential architecture. It is based on the Analog Discovery

2, a USB module that comprises the necessary power supplies, signal acquisition and signal generation circuitry.

The four-electrode method of impedance measurement avoids the adverse effects of the electrode impedance on the impedance plots and enables a better observation of the plant impedance. Increasing the distance between the measuring electrodes allows using a three-element –with a total of four parameters– equivalent circuit, which is convenient for data analysis. From those parameters, the resistance that models the extracellular fluid showed that it is consistently increasing with water loss –as recorded by means of the weight decrease. In contrast to other studies that place the electrodes into the plant stem, this study shows that water content can be measured on the leaves, where the hydration deficit might manifest earlier than in the plant stem in a living plant. However, such living-plant application needs of further development of suitable electrodes that do not disturb the plant physiology.

Acknowledgments

This work funded by the Institute of Scientific Research (IDIC) of the University of Lima (Perú) as part of the research project "*Medición en tiempo real de la Impedancia eléctrica para la detección de estrés hídrico en cultivos de espinaca*".

References

Asami, K., Yonezawa ', T., Wakamatsu ', H., Koyanagi ', N., 1996. Dielectric spectroscopy of biological cells, Bioelectrochemistry and Bioenergetics.

Barbosa, J.A., Freitas, V.M.S., Vidotto, L.H.B., Schleder, G.R., de Oliveira, R.A.G., da Rocha, J.F., Kubota, L.T., Vieira, L.C.S., Tolentino, H.C.N., Neckel, I.T., Gobbi, A.L., Santhiago, M., Lima, R.S., 2022. Biocompatible Wearable Electrodes on Leaves toward the On-Site Monitoring of Water Loss from Plants. ACS Appl Mater Interfaces. https://doi.org/10.1021/acsami.2c02943

Bar-On, L., Shacham-Diamand, Y., 2021. On the Interpretation of Four Point Impedance Spectroscopy of Plant Dehydration Monitoring. IEEE J Emerg Sel Top Circuits Syst 11, 482–492. https://doi.org/10.1109/JETCAS.2021.3098984

ben Hamed, K., Zorrig, W., Hamzaoui, A.H., 2016. Electrical impedance spectroscopy: A tool to investigate the responses of one halophyte to different growth and stress

conditions. Comput Electron Agric 123, 376–383. https://doi.org/10.1016/j.compag.2016.03.006

Comparini, D., Masi, E., Pandolfi, C., Sabbatini, L., Dolfi, M., Morosi, S., Mancuso, S., 2020. Stem electrical properties associated with water stress conditions in olive tree. Agric Water Manag 234. https://doi.org/10.1016/j.agwat.2020.106109

Dellis, J.-L., 2022. ZFit [WWW Document]. MATLAB Central File Exchange (https://es.mathworks.com/matlabcentral/fileexchange/19460-zfit).

Elsherbiny, O., Zhou, L., He, Y., Qiu, Z., 2022. A novel hybrid deep network for diagnosing water status in wheat crop using IoT-based multimodal data. Comput Electron Agric 203. https://doi.org/10.1016/j.compag.2022.107453

Garlando, U., Calvo, S., Barezzi, M., Sanginario, A., Motto Ros, P., Demarchi, D., 2022. Ask the plants directly: Understanding plant needs using electrical impedance measurements. Comput Electron Agric 193. https://doi.org/10.1016/j.compag.2022.106707

Grimnes, S., Martinsen, O.G., 2015. Bioimpedance and Bioelectricity Basics, 3rd Ed. Elsevier.

Hayden, R.I., Moyse, C.A., Calder, F.W., Crawford, D.P., Fensom, D.S., 1969. Electrical Impedance Studies on Potato and Alfalfa Tissue. J Exp Bot 20, 177–200. https://doi.org/10.1093/jxb/20.2.177

Hunt, E.R., Rock, B.N., Nobel, P.S., 1987. Measurement of Leaf Relative Water Content by Infrared Reflectance, REMOTE SENSING OF ENVIRONMENT.

Ibba, P., Crepaldi, M., Cantarella, G., Zini, G., Barcellona, A., Rivola, M., Petrelli, M., Petti, L., Lugli, P., 2021. Design and Validation of a Portable AD5933-Based Impedance Analyzer for Smart Agriculture. IEEE Access 9, 63656–63675. https://doi.org/10.1109/ACCESS.2021.3074269

Jamaludin, D., Abd Aziz, S., Ahmad, D., Jaafar, H.Z.E., 2015. Impedance analysis of Labisia pumila plant water status. Information Processing in Agriculture 2, 161–168. https://doi.org/10.1016/j.inpa.2015.07.004

Jócsák, I., Végvári, G., Vozáry, E., 2019. Electrical impedance measurement on plants: a review with some insights to other fields. Theor Exp Plant Physiol. https://doi.org/10.1007/s40626-019-00152-y

Kalyanaraman, A., Burnett, M., Fern, A., Khot, L., Viers, J., 2022. Special report: The AgAID AI institute for transforming workforce and decision support in agriculture. Comput Electron Agric 197. https://doi.org/10.1016/j.compag.2022.106944

Li, M.Q., Li, J.Y., Wei, X.H., Zhu, W.J., 2017. Early diagnosis and monitoring of nitrogen nutrition stress in tomato leaves using electrical impedance spectroscopy. International Journal of Agricultural and Biological Engineering 10, 194–205. https://doi.org/10.3965/j.ijabe.20171003.3188

Pethig, R., Kell, D.B., 1987. The passive electrical properties of biological systems: Their significance in physiology, biophysics and biotechnology. Phys Med Biol 32, 933–970. https://doi.org/10.1088/0031-9155/32/8/001

Prasad, A., Roy, M., 2020. Bioimpedance analysis of vascular tissue and fluid flow in human and plant body: A review. Biosyst Eng. https://doi.org/10.1016/j.biosystemseng.2020.06.006

Repo, T., Laukkanen, J., Silvennoinen, R., 2005. Measurement of the Tree Root Growth Using Electrical Impedance Spectro-scopy. Silva Fennica 39, 159–166. https://doi.org/http://dx.doi.org/10.14214/sf.380

Smart, R.E., Bingham, G.E., 1974. Rapid Estimates of Relative Water Content. Plant Physiol 53, 258–260.

Torres, I., Sánchez, M.T., Benlloch-González, M., Pérez-Marín, D., 2019. Irrigation decision support based on leaf relative water content determination in olive grove using near infrared spectroscopy. Biosyst Eng 180, 50–58. https://doi.org/10.1016/j.biosystemseng.2019.01.016

Watanabe, T., Ando, Y., Orikasa, T., Shiina, T., Kohyama, K., 2017. Effect of short time heating on the mechanical fracture and electrical impedance properties of spinach (Spinacia oleracea L.). J Food Eng 194, 9–14. https://doi.org/10.1016/j.jfoodeng.2016.09.001

Winter, H., Robinson, D.G., Heldt, H.W., 1994. Subcellular volumes and metabolite concentrations in spinach leaves.

Zhang, M.I.N., Willison, J.H.M., 1993. Electrical impedance analysis in plant tissues: impedance measurement in leaves. J Exp Bot 44, 1369–1375. https://doi.org/10.1093/jxb/44.8.1369

Zimmermann, D., Reuss, R., Westhoff, M., Geßner, P., Bauer, W., Bamberg, E., Bentrup, F.W., Zimmermann, U., 2008. A novel, non-invasive, online-monitoring, versatile and easy plant-based probe for measuring leaf water status. J Exp Bot 59, 3157–3167. https://doi.org/10.1093/jxb/ern171